Published in Journal of Applied Physics 80, issue 4, 2181-2186, 1996
which should be used for any reference to this work

A chemical state resolved x-ray photoelectron diffraction study: Initial stages in diamondlike carbon film deposition

R. G. Agostino,[a] O. M. Küttel, P. Aebi, R. Fasel, J. Osterwalder,[b] and L. Schlapbach
Institut de Physique, Université de Fribourg, Pérolles, CH-1700 Fribourg, Switzerland

The structural sensitivity of x-ray photoelectron diffraction is greatly enhanced by the acquisition of a full hemispherical diffraction pattern of chemically shifted core levels. Complex systems can be studied resolving the local order per element and per chemical environment. This technique is applied to study the earliest stages of hydrogenated diamondlike carbon film deposition on Si(001). Effects of the sample temperature and ion dose on the structure of deposited layers are discussed.

INTRODUCTION

Diamondlike carbon (DLC) films are mainly composed of a net of tetrahedrically coordinated C atoms.[1] Hardness, wear, thermal, and optical features are close to that of diamond films while their preparation is much less critical.[1] Using a mass and energy selected ion beam (MESIB) source,[2,3] it is possible to produce DLC films in ultrahigh vacuum (UHV) adjusting sample temperature, flux, incidence angle, and kinetic energy of the incoming ions. The production of Si:C, C:C, and C:H phases takes place in the first stages of DLC film deposition using hydrocarbon ions on Si substrates. The structure and thickness of these phases depends on deposition temperature and radical kinetic energy. SiC is found in amorphous and β-SiC phases, and C is found in amorphous sp^2 and sp^3 phases with eventual embedded diamond nuclei.[4] Different models predict that SiC plays the role of a supersaturated milieu in which the diamond is formed by thermal-spike induced precipitation.[5] However, a relation between the SiC structure at the beginning of the DLC film formation and diamond nuclei production and orientation is not established yet.

We have previously investigated diamond films produced by chemical vapor deposition, single-crystalline diamond, and highly oriented pyrolitic graphite, using conventional full hemispherical x-ray photoelectron diffraction (XPD) as well as other techniques.[6] In this article, we present a structural study of DLC films obtained by ion beam deposition of CH_n^+ (n=3,4) on Si(001) samples using MESIB source. The kinetic energies of the Mg K_α excited C1*s* and Si 2*p* photoelectrons, 970 and 1154 eV, respectively, are high enough to guarantee a direct interpretation of the XPD patterns.[7,8] Intensity maxima occur for emission angles corresponding to emitter–scatterer directions, atomic chains, or high density atomic planes. This phenomenon, known as *forward focusing*, makes the technique a unique structural tool which is able to probe the average local order around selected emitters near the surface. However, the application of XPD to DLC films is not straightforward. Usually, the films have an amorphous structure and different phases coexist by giving rise to a layered structure in which the stoichiometry varies continuously from the pure Si substrate to a hydrogenated C layer at the surface.[9–14] There are two main problems when applying the XPD technique to the investigation of the initial states of DLC growth: the emission from atoms in an amorphous phase results in a nonstructured XPD pattern and both the C and Si photoemission signals will carry information from different phases, i.e., Si:Si, Si:C, C:C, C:H.

The aim of this article is to show how a deeper insight can be gained when applying a fitting procedure to the core level signal in order to extract the diffraction patterns produced by single components. The structural sensitivity of conventional full hemispherical XPD is then improved by the possibility to explore the local order around a particular element in different chemical environments. In such a way we are able to study the interface formation and growth in thin film deposition where different chemical environments coexist. If one of the surface phases is ordered then the corresponding pattern shows diffraction features. On the other hand, amorphous layers have an unstructured pattern in which only a smooth dependence of the intensity on polar angle remains. However, the polar angle dependence of the averaged intensity of the chemically shifted component carries complementary information on the depth distribution of the chemical species in the film/interface system.

Therefore, we explore the C:Si-, C:C-, and C:H-rich phases for the C atoms and the pure Si substrate and the Si:C-rich phase for the Si atoms. It is shown how the structure of the buried Si(001) surface, of the SiC interlayer, of the C-rich phases and the depth distribution of the different phases can be characterized. Measurements done as a function of temperature are presented.

EXPERIMENT

The deposition and analysis system is based on a modified Vacuum Generator ESCALAB Mark II spectrometer[15] with a base pressure of 2×10^{-11} mbar, equipped with a three channeltron hemispherical electron energy analyzer, a Mg K_α and Si K_α twin anode x-ray source, a quadrupole mass spectrometer, and a low energy electron diffraction (LEED) system.

[a]Author to whom all correspondence should be addressed; Electronic mail: raffaele.agostino@unifr.ch
[b]Permanent address: Physik-Institut, Universität Zürich-Irchel, Winterhurerstrasse 190, CH-8057 Zürich, Switzerland.

During deposition and analysis the sample is mounted on a five-axis manipulator. Rotations are computer controlled such that the photoelectron emission angles θ (polar angle, with respect to the normal) and ϕ (azimuthal angle) can be swept over the whole hemisphere above the sample and a series of spectra can be recorded automatically on a predetermined set of angles (θ,ϕ). The experimental procedure consists in the acquisition of the Mg K_α excited, C 1*s* and Si 2*p* x-ray photoelectron spectra for each (θ,ϕ) setting. Up to 8000 spectra are recorded with a pass energy of 20 eV such that the energy resolution is practically only determined by the intrinsic width of Mg K_α radiation. In order to extract the chemically shifted components, a Shirley background is removed from each spectrum and the emission line is approximated by (up to 3) least-squares fitted Gaussian curves whose centers and full widths at half-maximum are kept constant. The integral of each Gaussian curve is extracted as the intensity of the chemically shifted component. The intensity maps, $I(\theta,\phi)$, are stereographically projected using a linear grey scale representation.[15] Normal emission appears in the center while grazing emission is plotted toward the border.

The MESIB source is mounted directly on the analysis system with the focus position identical to the one of the electron energy analyzer used in XPD. The source allows a minimum energy of 5–10 eV, masses up to 2000 a.m.u., is UHV compatible, and has a mass resolution of unity. Details of the MESIB source are described elsewhere.[2] Deposition was performed using a CH_n^+ $(n=3,4)$ beam at 120 eV. The pressure of the system rises to the 10^{-9} mbar range during deposition. The *p*-doped Si(001) samples were cleaned by means of Ar^+ ion sputtering and annealing (1050 K) procedures. The sample temperature was controlled by resistive heating. Surface cleanliness and order were checked by x-ray photoelectron spectroscopy (XPS) and LEED, respectively. Very low C contamination (<2% of a monolayer) was present while no O, Ar, or other contaminants were detected.

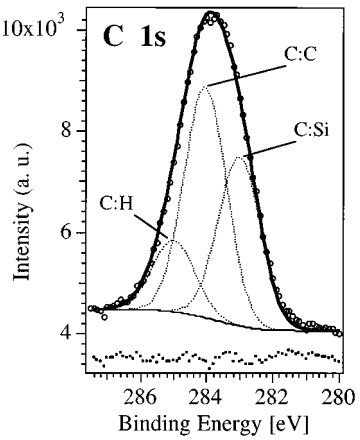

FIG. 1. Typical Mg K_α radiation (1253.6 eV) excited C 1*s* emission spectrum from a hydrogenated carbon film deposited on Si(001) at 670 K. The C:Si, C:C, and C:H components have binding energies of 282.9, 284.1, and 285.0 eV, respectively. The raw data are shown as an open circle, the fitting curve as a thick line, the Shirley background as a thin line, the line components as dotted curves, and the difference between data and fit as dots.

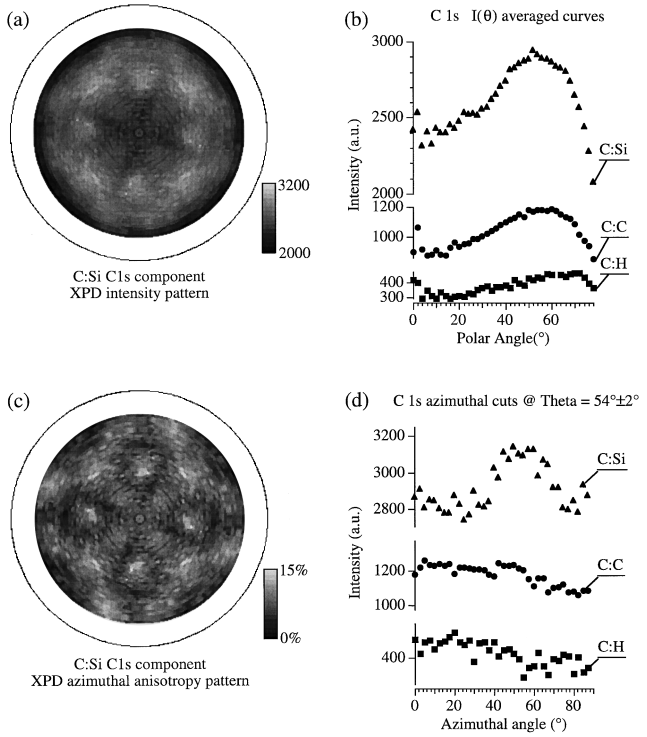

FIG. 2. (a) Stereographic projection of the diffraction patterns from the C:Si C 1*s* component of a DLC film obtained by depositing 16.8×10^{15} ions/cm^{-2} at 670 K and subsequently annealing at 1070 K for 10 min. Only one-fourth of the solid angle above the sample surface is measured. The figure is obtained by exploiting the fourfold symmetry of the system previously verified by the acquisition of azimuthal scans. (b) Polar angle dependence of the different azimuthally averaged C 1*s* components. (c) C:Si azimuthal anisotropy pattern (see the text). The data representation uses a linear gray scale ranging from 0 (black) to the maximum anisotropy (white). (d) Azimuthal scans extracted from the patterns of the different C 1*s* components. The azimuthal scans are taken at a polar angle of 54°±2°. The maximum of the C:Si intensity at the azimuthal angle of 55° corresponds to the [111] direction in the SiC lattice.

RESULTS AND DISCUSSION

As can be clearly seen in Fig. 1, the C 1*s* line from a hydrogenated carbon film deposited on Si(001) contains different components. In C:Si, C:C, and C:H phases, C 1*s* emission will result at increasing binding energies,[16] i.e., at 282.85±0.15, 284.05±0.15, and 285.05±0.30 eV, respectively. It is not possible to distinguish sp^2 from sp^3 bonded C atoms because binding energies are very similar.[16] A systematic error in the fitting procedure can arise from the presence of mixed bonding in which C atoms have a chemical environment corresponding neither to the SiC phase nor to C clusters. This gives rise to errors in the evaluation of the components binding energies, and the fact that the energy separation between the C:C component and the C:Si component is lower than that found in the literature[16] agrees with this picture. Nevertheless, a decomposition of the line shape into three Gaussian curves permits us to follow the average variation in the surface chemistry as a function of temperature and ion dose.

In Fig. 2(a) we show the chemically resolved C 1*s* XPD pattern for the C:Si component. In this case the film was deposited at 670 K with an ion dose of 16.8×10^{15} ions cm^{-2}

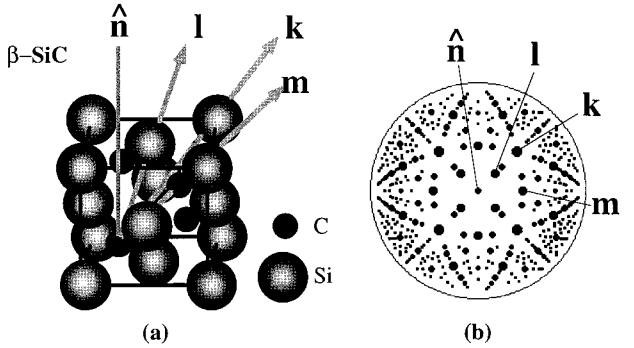

FIG. 3. (a) Schematic representation of the directions of the principal scattering paths starting from a C atom in a SiC unit cell. The directions **l** and **k** are connecting the C atom with Si atoms at the center and at the corner of the upper surface in the unit cell, respectively. Their polar angles are 25° (**k**) and 54° (**l**) with respect to the normal $\hat{\mathbf{n}}$ while they have the same azimuth. Direction **m** connects two C atoms and has a polar angle of 45° with respect to the normal $\hat{\mathbf{n}}$. Note that it is also rotated by 45° with respect to directions **k** and **l**. (b) Stereographic projection of the scattering path directions in a SiC lattice. The dot size is inversely proportional to the emitter–scatterer distance. Directions $\hat{\mathbf{n}}$, **k**, **l**, and **m** are indicated.

and subsequently annealed at 1070 K for 10 min. Generally, two kinds of anisotropies are present in the patterns: (a) the average polar anisotropy which is mainly related to the depth profile of the emitting species (see below) and (b) the azimuthal anisotropy which results from the atomic order in the sampled region. In Fig. 2(b), we depict the azimuthally averaged polar dependence of the three components. Normalizing the intensity of each azimuth at a fixed polar angle to its mean value, i.e., to the values of curve 2(b), we obtain the azimuthal anisotropy pattern shown in Fig. 2(c). The C:C and C:H azimuthal anisotropy patterns are flat as it is expected for amorphous phases. In Fig. 2(d), comparing the azimuthal anisotropy of the different components at a fixed polar angle, we show that no anisotropy is present in the C:C and C:H curves.

In the C:Si C 1*s* pattern of Fig. 2(c) we find diffuse diffraction maxima which correspond to the first and second nearest-neighbor atom directions in a diamond or zinc-blende lattice epitaxially grown on the Si substrate. The anisotropy, defined as $(I_{\max}-I_{\min})/I_{\max}$, of the pattern is 10.5% along the polar angle of 54° [Fig. 2(d)]. The experimental value[8] of anisotropy for the same polar angle on SiC single crystals is 43%. From the values in our experiment we can conclude that in the C:Si phase local zinc-blende order coexists with amorphous regions, therefore having a coexistence of β-SiC(001) clusters on Si(001) with an amorphous SiC phase. In Fig. 3 the directions $\hat{\mathbf{n}}$**, l, k, m** appearing in a SiC unit cell [Fig. 3(a)] are mapped into the stereographic projection [Fig. 3(b)] to be compared with Fig. 2(c). In Fig. 3(b) many so-called forward focusing directions are marked with a marker size inversely proportional to the corresponding atom–atom distance. Some of these forward scattering directions only appear above a certain thickness of the layer. We estimate the thickness of the β-SiC layer in Fig. 2(c) to be smaller than 5 Å on average, because there is no forward focusing maximum along normal emission. Such a forward focusing maximum is expected for a thickness greater than one unit cell where two or more atoms are sitting on top of each other.

The polar angle dependence of the azimuthally averaged intensity from the three patterns [Fig. 2(b)] can be related to the depth distribution of the emitting species. An elementary model[17] can be drawn taking into account the inelastic losses experienced by the photoelectron in the solid and neglecting, as a second-order effect, the inelastic mean free path (λ) dependence on the species concentration. For simplicity, it is also assumed that a particular species is located within a depth interval with constant concentration. In this model, the emitted intensity of one species as a function of polar angle is given by:

$$I(\theta)\propto\int_{z_i}^{z_f}\exp\left(-\frac{z}{\lambda\,\cos(\theta)}\right)dz$$
$$=\lambda\,\cos(\theta)\left[\exp\left(-\frac{z_f}{\lambda\,\cos(\theta)}\right)-\exp\left(-\frac{z_i}{\lambda\,\cos(\theta)}\right)\right],$$

where the species is located within an interval z_i, z_f (Fig. 4).

On the other hand the sample area seen by the analyzer varies with $\cos(\theta)^{-1}$ so that the final angle polar dependence of the intensity is:

$$I(\theta)\propto\lambda\left[\exp\left(-\frac{z_f}{\lambda\,\cos(\theta)}\right)-\exp\left(-\frac{z_i}{\lambda\,\cos(\theta)}\right)\right].$$

An example of depth profile evaluation through the $I(\theta)$ curves is given in Fig. 4 where the systematic evolution of the calculated, azimuthally averaged intensity as a function of polar angle for different thickness distributions [Fig. 4(a) and 4(b)] is shown together with the polar angle dependence of the experimental patterns for a hydrogenated C layer [Fig. 4(c)]. The calculated curves fit very well the experimental $I(\theta)$ [the dotted curves in Fig. 4(c)]. This makes it clear that we can get a qualitative depth profile where the values of initial and final depth (z_i^A and z_f^A) found by a fitting procedure can be related to the near surface depth interval with a given species *A*. The fit performed on the azimuthally averaged intensity curves of Fig. 4(d) indicates that the C:Si is thickest, extending from the surface down to 19.5 Å (λ=16.0 Å), while the C:C phase ranges from 1.4 to 6.2 Å, and the hydrogenated C layer, between 1.6 and 3.4 Å, is closest to the surface. From these results we find that Si from the C:Si phase extends up to close to the surface containing the C:C phase. This is consistent with the subplantation model.[13] The very surface is H rich with the presence of a high fraction of C:C bonding.

The Si 2*p* XPS emission line (Fig. 5) can be separated into a Si:Si (bulk) and a Si:C component. The former is centered at 99.20±0.10 eV in binding energy while the latter is at 100.00±0.20 eV. The total intensity Si 2*p* XPD pattern derived from a complete set of Si 2*p* spectra recorded after an ion dose of 9.4×10^{15} ions cm^{-2} deposited on the Si(001) at 670 K is shown in Fig. 6(a). It is similar to the one of clean Si(001) (not shown), with the difference that features in Fig. 6(a) are slightly smeared out and intensity decreases

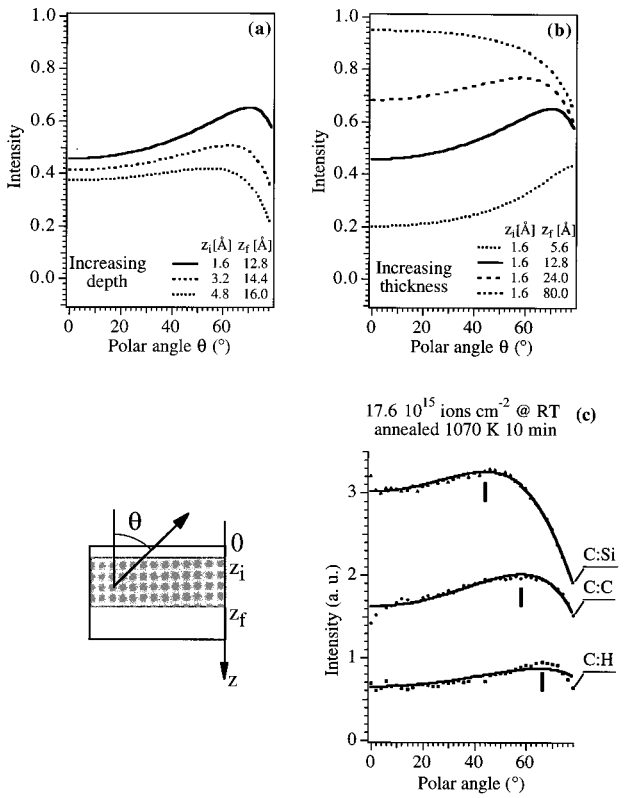

FIG. 4. (a) Calculated emission intensity vs polar angle curves for an emitting species confined in a buried layer ranging from z_i to z_f (see the text). The density of the species in the buried layer is assumed constant. The depth values are calculated assuming an inelastic mean free path (λ) value of 16 Å. Curves are calculated for a layer with fixed thickness (11.2 Å) and increasing depth z_i. Note that with increasing depth the intensity maximum shifts toward lower polar angle. (b) Calculated emission intensity curves for increasing layer thickness with fixed depth (z_i=1.6 Å). Note that thicker layers have intensity maxima at lower polar angle. The emission intensity from a very thick layer (z_i=1.6 Å, z_f=80 Å) has a maximum at normal emission. (c) Experimental polar angle dependence of the azimuthally averaged C 1*s* components from a hydrogenated carbon film deposited on Si(001) at RT (dotted curve). The film was annealed for 10 min at 1070 K. The solid line is obtained by fitting. The maxima for each curve are marked by a vertical tick.

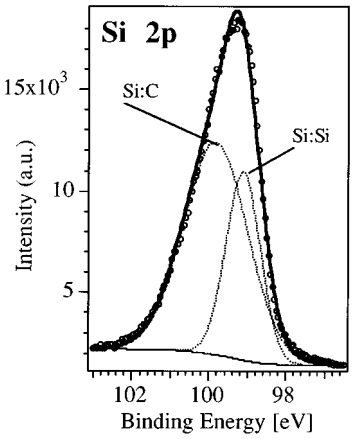

FIG. 5. Typical Mg K_α radiation (1253.6 eV) excited Si 2*p* emission spectrum from a hydrogenated carbon film deposited on Si(001), at 670 K. The Si:Si and Si:C components have binding energies of 99.2 and 100.0 eV, respectively. The raw data are shown as an open circle, the fitting curve as a thick line, the Shirley background as a thin line, and the line components as dotted curves.

faster with polar angle. This is consistent with the presence of a layer with a different structure on top of the ordered Si structure. No other information can be extracted from the pattern concerning the differences between the two phases of pure Si and Si:C hidden in the Si 2*p* emission line. This kind of information is obtained now by splitting the signal into the chemically resolved diffractograms shown in Figs. 6(b) and 6(c). Like the Si 2*p* total intensity pattern, the signal coming from the Si:Si component is similar to that of clean Si(001) except for a faster decrease of intensity with polar angle. Comparing this with clean Si(001) experimental patterns we find that the anisotropy is quite high, varying from 25% for [111]-like directions to 34% along the normal. Thus the Si(001) buried surface is well ordered. On the other hand, the diffraction pattern of the Si:C component of the Si 2*p* line [Fig. 6(b)] exhibits broader structures and a different intensity versus polar angle behavior. We can distinguish some forward focusing maxima which are located along forward scattering directions of the zinc-blende structure. In this pattern the anisotropies are low, varying from 6% along the surface normal to 12% along the [011]-like directions, showing the coexistence of amorphous and ordered SiC. We deduce that this Si:C pattern, like the C:Si pattern derived from the C 1*s* emission [Fig. 2(a)], is related to epitaxial β-SiC(001) clusters on top of the Si(001) substrate coexisting with a disordered SiC phase. It is worth noting that the SiC structure is effectively revealed from both the C 1*s* *and* Si 2*p* *carbide* components. The azimuthally averaged intensity, $I(\theta)$, of the Si:C component [Fig. 6(d)] increases from normal emission up to θ=58° and then slowly decreases while the Si:Si component shows a maximum at normal emission. A fit within the model of layers of constant composition performed for the Si:C and Si:Si phases gives emitting regions ranging from 1.8 to 11.0 Å and from 5.7 Å into the bulk, respectively.

A series of similar C 1*s* and Si 2*p* chemically resolved patterns were recorded for Si(001) samples at different ion doses and substrate temperatures. For the first stage of hydrogenated DLC film growth a nonstructured Si:Si pattern indicates that upon CH_n^+ deposition at room temperature (RT), the Si(001) surface is amorphized by sputtering effects. At higher temperatures (670 and 790 K) the diffusion process allows a reordering of the lattice and the Si(001) bulk diffraction pattern is recovered. From the very beginning of the deposition process a SiC interlayer is formed. Thickness and crystallinity are strictly dependent on the deposition temperature: at RT, layers are amorphous (Si:C Si 2*p* and C:Si C 1*s* component patterns are structureless) and thin while at higher temperatures they show the presence of an epitaxial β-SiC(001) coexisting with a thicker amorphous SiC layer as in the cases shown in Figs. 2 and 6. The ordering process does not involve the C:C phase which has a disordered nature for all the deposition temperatures and ion doses investigated so far. Furthermore, following the C:H C 1*s* component intensity as a function of temperature we find

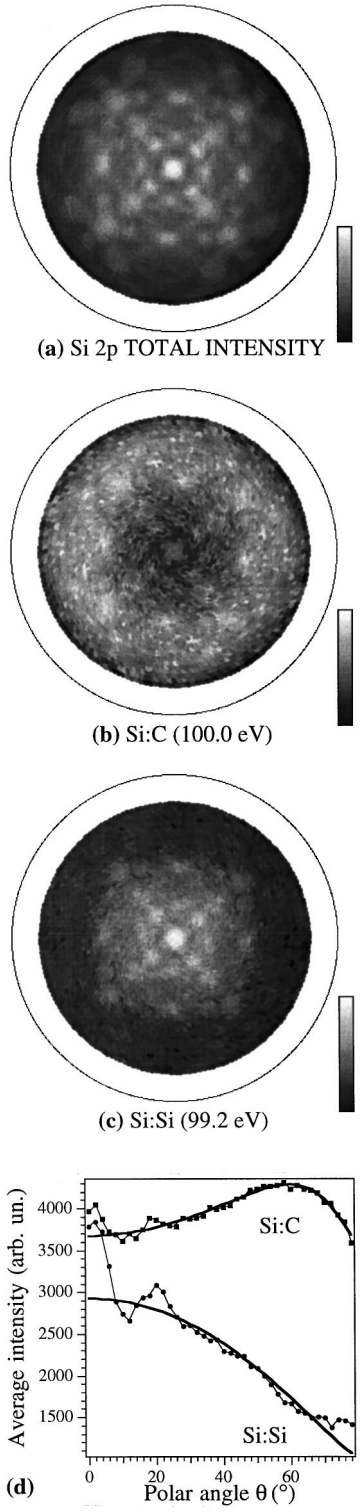

FIG. 6. Stereographic projection of the Si 2*p* XPD patterns from a hydrogenated carbon film deposited on Si(001) at 670 K. The patterns are folded exploiting the four-fold rotational symmetry of the system. (a) The total intensity Si 2*p* XPD pattern in which both *pure* silicon and carbide contributions are present. Diffraction patterns of the Si:Si (b) and Si:C (c) Si 2*p* components extracted by the fitting procedure (see the text). No smoothing procedure is applied to the data. (d) Polar angle dependence of the azimuthally averaged intensity of the components. Solid lines are drawn as a guide to the eye to point out the different behavior.

that the H atoms bound to C are incorporated in the film at RT while only one-fourth of them remain close to the surface at high temperature. This is consistent with other experiments[4] and theoretical works.[18] The C:H component is systematically less intense than the other two. Nevertheless, it is necessary to include it in the fitting procedure of all the patterns in order to minimize the value of χ^2. In all cases the C:H C patterns did not show any diffraction features.

CONCLUSIONS

We have presented a chemical state resolved study of DLC film by means of an extension of conventional full hemispherical XPD. By extracting the diffraction patterns corresponding to several chemically shifted components of the core levels, we can describe the local order of different phases coexisting in proximity of the surface. Moreover we reported on the development of the initial stages of the DLC film formation on a crystalline Si substrate as a function of ion dose and temperature.

ACKNOWLEDGMENTS

We gratefully acknowledge the excellent technical support of O. Raetzo, E. Mooser, H. Tschopp, and F. Bourqui, One of the authors (R.G.A.) has been supported by the EC training project (Contract No. ERBCHBICT 941026).

[1] S. R. Kasi, Y. Lifshitz, J. W. Rabalais, and G. Lempert, Angew. Chem. **100**, 1245 (1988); J. J. Cuomo, J. P. Dole, J. Bruley, and J. C. Liu, Appl. Phys. Lett. **58**, 466 (1991); S. R. Kasi, H. Kang, and J. W. Rabalais, Phys. Rev. Lett **59**, 75 (1987).
[2] O. M. Küttel, P. Groening, R. G. Agostino, and L. Schlapbach, J. Vac. Sci. Technol. A (in press).
[3] Y. Lifshitz, G. D. Lempert, E. Grossman, I. Avigal, C. Uzan-Saguy, R. Kalish, J. Kulik, D. Marton, and J. W. Rabalais, Diam. Relat. Mater. **4**, 318 (1995), and references therein.
[4] S. Sattel, M. Weiler, J. Gerber, T. Giessen, H. Roth, M. Sheib, K. Jung, H. Ehrhardt, and J. Robertson, Diam. Relat. Mater. **4**, 333 (1995).
[5] B. R. Stoner, G. H. M. Ma, S. D. Wolter, and J. T. Glass, Phys. Rev. B **45**, 11 067 (1992).
[6] R. G. Agostino, O. M. Küttel, R. Fasel, J. Osterwalder, and L. Schlapbach, Phys. Rev. B **49**, 13 820 (1994); O. M. Küttel, R. G. Agostino, R. Fasel, J. Osterwalder, and L. Schlapbach, Surf. Sci. **312**, 131 (1994); O. M. Küttel, J. Osterwalder, L. Schlapbach, and R. G. Agostino, Diam. Relat. Mater. **2**, 548 (1993).
[7] J. Osterwalder, P. Aebi, R. Fasel, D. Naumovic, P. Schwaller, T. Kreutz, L. Schlapbach, T. Abukawa, and S. Kono, Surf. Sci. **331–333**, 1002 (1995), and references therein.
[8] S. Juillaguet, L. Kubler, M. Diani, J. L. Bischoff, G. Gewinner, P. Wetzel, and N. Bécourt, Surf. Sci. **339**, 363 (1995).
[9] W. M. Lau, I. Bello, X. Feng, L. J. Huang, Q. Fuguang, Y. Zhenyu, and R. Zhy Zhang, J. Appl. Phys. **70**, 5623 (1991).
[10] Y. Lifshitz, G. D. Lempert, S. Rotter, I. Avigal, C. Uzan Saguy, R. Kalish, J. Kulik, D. Marton, and J. W. Rabalais, Diam. Relat. Mater. **3**, 542 (1994).
[11] J. Kulik, Y. Lifshitz, G. D. Lempert, J. W. Rabalais, and D. Marton, J. Appl. Phys. **76**, 5063 (1994).
[12] X. He, W. Li, and H. Li, J. Vac. Sci. Technol. A **11**, 2964 (1993).
[13] Y. Lifshitz, S. R. Kasi, J. W. Rabalais, and W. Ekstein, Phys. Rev. B **41**, 10 468 (1990).
[14] E. Schaller, O. M. Küttel, P. Aebi, and L. Schlapbach, Appl. Phys. Lett. **67**, 1533 (1995).
[15] J. Osterwalder, T. Greber, A. Stuck, and L. Schlapbach, Phys. Rev. B **44**, 13 764 (1991).

[16] D. N. Belton and S. J. Schmieg, J. Vac. Sci. Technol. A **8**, 2353 (1990).

[17] A complete description of the polar angle dependence of the azimuthally averaged intensity has to take into account a refraction term (inner potential effect). We do not treat this term here because refraction becomes only important at high polar angle and low kinetic energies of the outgoing electrons.

[18] S. Uhlmann, T. Frauenheim, and U. Stephan, Phys. Rev. B **51**, 4541 (1995); S. Uhlmann and T. Frauenheim, Diam. Relat. Mater. (to be published).